Inorganic Chemistry

Article

pubs.acs.org/IC

1,2,4-Triazolyl-Carboxylate-Based MOFs Incorporating Triangular Cu(II)-Hydroxo Clusters: Topological Metamorphosis and Magnetism

Sergiy I. Vasylevs'kyy,[†] Ganna A. Senchyk,[†] Andrey B. Lysenko,*[,†] Eduard B. Rusanov,[‡] Alexander N. Chernega,[‡] Julia Jezierska,[§] Harald Krautscheid,[∥] Konstantin V. Domasevitch,[†] and Andrew Ozarowski*[,⊥]

[†]Inorganic Chemistry Department, Taras Shevchenko National University of Kyiv, Volodimirska Street 64, Kyiv 01033, Ukraine

[‡]Institute of Organic Chemistry, 02660, Murmanska Street 5, Kyiv, Ukraine

[§]Faculty of Chemistry, University of Wroclaw, 14 Joliot-Curie Str., 50-383 Wroclaw, Poland

[∥]Institut für Anorganische Chemie, Universität Leipzig, Johannisallee 29, D-04103 Leipzig, Germany

[⊥]National High Magnetic Field Laboratory, Florida State University, 1800 East Paul Dirac Drive, Tallahassee, Florida 32310, United States

Supporting Information

ABSTRACT: Bifunctional 1,2,4-triazole-carboxylate ligands, an achiral 1,2,4-triazol-4-yl-acetic acid (**trgly-H**) and a chiral (*d*)-2-(1,2,4-triazol-4-yl)-propionic acid (*d*-**trala-H**), derived from the corresponding α-amino acid precursors revealed unique binding abilities in the construction of Cu(II)-coordination polymers composing discrete triangular [$Cu_3(\mu_3$-OH)] clusters. A related series of MOFs, [$Cu_3(\mu_3$-OH)(**trgly**)$_3(SO_4)$]·$2H_2O$ (**1a**), [$Cu_3(\mu_3$-OH)(**trgly**)$_3(H_2O)_3$]SO_4·$16H_2O$ (**1b**), $Cu_3(\mu_3$-OH)(*d*-**trala**)$_3(ClO_4)_{0.5}](ClO_4)_{1.5}$·$1.5H_2O$ (**2**), was prepared, and their crystal structures were determined by means of X-ray diffraction. Being singly deprotonated, the organic ligands act as multidentate μ_3- or μ_4-donors using *tr* and $-COO^-$ moieties. The generated [$Cu_3(\mu_3$-OH)$(tr)_3$] cluster core is primarily supported by three [-N-N-] triazole heterocycles in a basal plane and tripodal-assisted μ_3-anions (SO_4^{2-}: **1a**; ClO_4^-: **2**) capping the axial faces. The carboxylate groups join the units into either two-dimensional (2D) layer (**1a**, **2**) or 3D zeolite-like networks (**1b**). Compound **1b** represents the topology of α-Po (pcu: $4^{12}.6^3$) and crystallizes in the noncentrosymmetric space group $I\bar{4}3m$, in which the six-connected [$Cu_3(\mu_3$-OH)] clusters and **trgly** self-assemble in an open-channel cubic array possessing ~56% solvent-accessible volume. Upon slight thermal treatment (~60 °C), the structure irreversibly shrinks to the nonporous 2D motif **1a** that belongs to a uninodal (3,6) network type. In structure **2** (space group $R3_2$), due to the [-N-N-] triazole and 1,3-bidentate carboxylate binding mode, each organic ligand bridges three metal clusters affording cross-linking of two adjacent layers with the same (3,6) topology. The resultant 3,9-c net is novel and can be categorized as two-nodal with point symbol $\{4^{18}.6^{18}\}\{4^2.6\}_3$. Spin frustration and antisymmetric exchange effects, resulting in abnormally low *g* values in the S = 1/2 states, were observed in the magnetic properties and the EPR spectra.

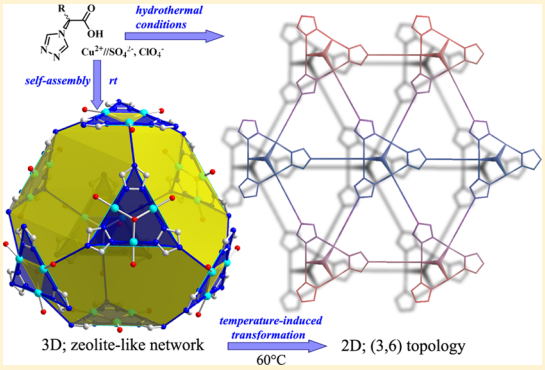

INTRODUCTION

Metal organic frameworks (MOFs) incorporating trinuclear hydroxoclusters [$Cu_3(\mu_3$-OH)] have received intensive research interest for multiple applications in gas storage and sorption,[1] catalysis (like peroxidative oxidation of alkanes,[2] CO oxidation,[3] etc.) and magnetism (e.g., to test magnetic exchange models in spin-frustrated systems,[4] or for spin-canted ferro- and antiferromagnetism[5]). Their structure and redox properties make them attractive models for the active sites of biomolecules, like the multicopper oxidases.[6] In this sense, 1,2,4-triazole (*tr*) derivatives are a unique family of N-donor building blocks which provide a short [-N-N-] linkage between two metal centers to achieve the molecular triangular topology.[7] Deprotonation of a N−H triazole function induces an important structural evolution in the molecular assemblies connecting the triangular motifs into three-dimensional (3D) coordination arrays through three angularly arranged basal binding sites (Scheme 1: a, b).[8] For these purposes, employing bi- or multitopic triazole ligands which bear various additional donor moieties (e.g., *py*, carboxylate) seems to be a promising approach for designing solids. In this regard, the mixed-donor triazolyl-carboxylate ligands as well as their complexes are subjects of extensive interest.[9] Both functions belonging to a particular class of cluster-supporting and self-complementary bridges, show high binding efficiency in fabrication of heteroleptic triazole(ate) and carboxylate complexes.[8c,10] The major advantage of 1,2,4-triazolyl-carboxylates lies in the

Received: December 26, 2013
Published: March 18, 2014

   dx.doi.org/10.1021/ic403148f | *Inorg. Chem.* 2014, 53, 3642−3654

Scheme 1. (a) Trinuclear Hydrocluster $[Cu_3(\mu_3\text{-}OH)(tr)_3]$; (b) a Self-Assembly of $[Cu_3(\mu_3\text{-}OH)(tr)_3]$ Clusters in a 3D Cubic Array; (c) 1,2,4-Triazolylcarboxylic Acids Explored in This Paper: the Presence of CH_3-Group at the α-Position of trala-H Was Aimed to Elucidate Its Influence on the Coordination Network Topology; (d) the Binding Mode Was Observed for $[Cu_3(\mu_3\text{-}O)(trgly)_3(H_2O)_3]BF_4{\cdot}H_2O$[11]

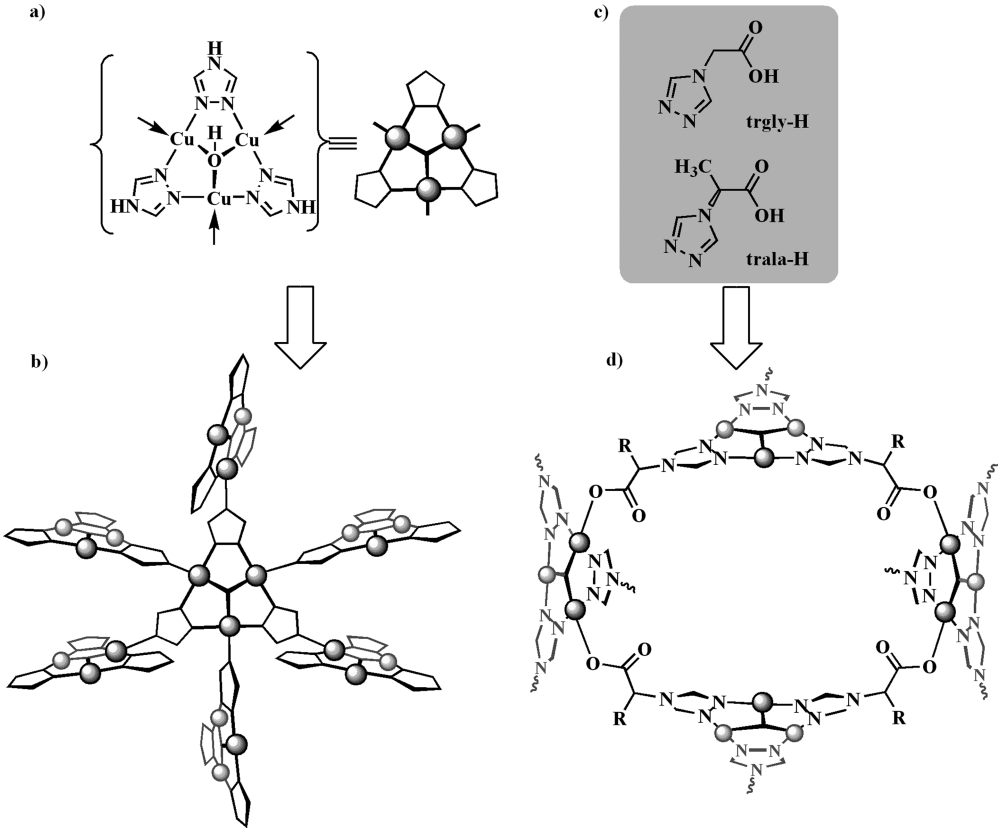

possibility of diverse ligand design reflected in a practical and reliable synthesis through commercial or readily accessible precursors. Among them, natural amino acids reveal an almost unexplored library of molecular building blocks with desirable side-chain functionality. The aspect of native chirality at tertiary carbon centers in such molecules opens a straightforward pathway to homochiral coordination polymers. In a pioneering work, Garcia et al. successfully applied a simple 1,2,4-triazole derivative of glycine (1,2,4-triazol-4-yl-acetic acid) to engineer a microporous zeolite-like framework based on $[Cu_3(\mu_3\text{-}OH)]$ scaffolds for gas sorption application (Scheme 1: c, d).[11]

Recently Lässig, Lincke, and co-workers demonstrated another attractive feature of 1,2,4-triazolyl-carboxylates concerning the topological transformation of the molecular complexes and low dimensional polymeric precursors into the interpenetrated 3D frameworks through simple thermal conversion.[12] Even more recently,[13] reversible crystal-to-amorphous-like phase transformation of the porous 3D framework consisting of triangular $[Cu_3(\mu_3\text{-}OH)(\mu_2\text{-}O)(tr)_2]$ clusters was reported by Xia et al. Exploiting the solid-state approach can lead to coordination solids with a sensory magnetic response, especially interesting in context of novel magnetic materials.

In this report, we describe the coordination abilities of bifunctional 1,2,4-trizolyl-carboxylate ligands (**trgly-H**, *d*-**trala-H**) derived from glycine and (*d*)-alanine toward rational construction of $[Cu_3(\mu_3\text{-}OH)]$-based MOFs exhibiting diverse topologies and tending to form solvatomorphs.

EXPERIMENTAL SECTION

Caution! *Since $Cu(ClO_4)_2{\cdot}6H_2O$ and compound* **2** *are potentially explosive, they must be handled with extreme care.*

Synthesis of the Organic Ligands. All chemicals were of reagent grade and used as received without further purification. The organic ligands were prepared in moderate yields up to 30% using the general method normally applied for aromatic and heterocyclic amines: refluxing of the corresponding amino acid (gly or (*d*)-ala) with *N*,*N*-dimethylformamide azine in toluene in the presence of $TsOH{\cdot}H_2O$.[14] The workup procedure with isolation of the potassium intermediates (**trgly-K** and **trala-K**) was found to be convenient and general because of the highly soluble nature of 1,2,4-triazolyl-carboxylates.

1,2,4-Triazol-4-yl-acetic Acid, ***trgly-H.*** In a typical procedure,[14] a mixture of *gly* (4.88 g, 0.0650 mmol), *N*,*N*-dimethylformamide azine (13.85 g, 0.0974 mmol) and $TsOH{\cdot}H_2O$ (0.520 g, 2.73 μmol) in toluene (15 mL) was stirred under reflux for 36 h (the reaction was monitored by evolution of dimethylamine). After being cooled to rt, the solvent was decanted, and the dark viscous residue was dissolved in hot ethanol (30 mL). To the dark solution was added an ethanolic (20 mL) solution of KOH (7.28 g, 0.129 mmol) that afforded a pale-yellow precipitate of potassium 1,2,4-triazol-4-yl-acetate, **trgly-K**. The solid was filtered off, washed with small portions of ethanol (3 × 5 mL). The white precipitate was redissolved in ethanol, and then 9.1 M hydrogen chloride in ethanol was added, adjusting the pH to 4. The resulting white precipitate of KCl was filtered off. The filtrate was concentrated *in vacuo* to a volume of 4 mL that led to the desired white product (2.56 g, 31%). A second crop of the product was not isolated from the remaining syrup. Anal. for **trgly-H·0·5H$_2$O**, $C_4H_6N_3O_{2.5}$. Calc (%): C, 35.30; H, 4.44; N, 30.87. Found (%): C, 35.10; H, 4.54; N, 30.65. ^{1}H NMR (400 MHz, DMSO-d_6: CCl_4 = 1: 3,

dx.doi.org/10.1021/ic403148f | Inorg. Chem. 2014, 53, 3642−3654

TMS): δ = 8.32 (2 H, s, *tr*), 4.79 (2 H, s, -CH_2-). IR (KBr pellet, cm^{-1}): 422s, 630m, 666s, 786s, 882m, 894m, 958m, 976m, 1012s, 1080m, 1198s, 1240s, 1348s, 1384m, 1428w, 1456m, 1524s, 1544s, 1652w, 1732s, 1942m, 2730w, 2816w, 2858w, 2942w, 2994m, 3062w, 3124s, 3148m, 3420w.

*(d)-2-(1,2,4-Triazol-4-yl)propionic Acid, (d)-**trala-H**.* In a typical procedure,[14] a mixture of (*d*)-*ala* (4.45 g, 0.0499 mmol), *N,N*-dimethylformamide azine (10.65 g, 0.0748 mmol) and TsOH·H_2O (0.400 g, 2.73 μmol) in toluene (15 mL) was stirred under reflux for 40 h. After being cooled to rt, the solvent was decanted, and the dark viscous residue was dissolved in hot ethanol (20 mL). To the dark solution was added an ethanolic (20 mL) solution of KOH (5.60 g, 0.100 mmol) that gave a pale-yellow precipitate of potassium 1,2,4-triazol-4-yl-propionate, **trala-K**. The solid was filtered off, washed with small portions of ethanol (3 × 5 mL), and then redissolved with stirring in 30 mL of hot ethanol (60 °C). To the solution was added 9.1 M hydrogen chloride in ethanol, adjusting the pH to 4. The resulting white precipitate of KCl was then removed by filtration. Partial evaporation of the solvent *in vacuo* to a volume of 3 mL left a white solid, which was isolated and dried at 70 °C giving the desired product (1.90 g, 27%). Anal. for $C_5H_7N_3O_2$. Calc (%):C, 42.55; H, 5.00; N, 29.77. Found (%): C, 42.47; H, 5.11; N, 29.60. ^{1}H NMR (400 MHz, DMSO-d_6: CCl_4 = 1: 3, TMS): 8.57 (2 H, *tr*), 5.21 (1H, q, *J*=7.1 Hz, *CH*), 1.83 (3H, d, *J*=7.1 Hz, CH_3). IR (KBr pellet, cm^{-1}): 448w, 544w, 578w, 628s, 678s, 730m, 796m, 848s, 884s, 948m, 984m, 1034s, 1066s, 1096s, 1192s, 1220s, 1256s, 1286s, 1314s, 1380m, 1404m, 1462m, 1544s, 1674m, 1732s, 2802w, 2826w, 2884w, 2912w, 2948w, 2974m, 2998w, 3110w, 3136s.

Synthesis of the Coordination Compounds. *[$Cu_3(\mu_3$-OH)-(trgly)$_3$(SO_4)]·2H_2O (**1a**).* A mixture of $CuSO_4$·5H_2O (50.0 mg, 0.200 mmol), **trgly-H·0.5H_2O** (27.2 mg, 0.200 mmol), and 5 mL of water were placed in a 20 mL Teflon-lined steel autoclave, stirred for 10 min at rt, and then heated at 120 °C for 36 h. Cooling to rt during the next 60 h led to green-blue prisms of the product that were collected, washed with water, and dried in air. Yield 28.7 mg (60%). Anal. Calc for $C_{12}H_{17}Cu_3N_9O_{13}S$ (%): C, 20.07; H, 2.39; N, 17.56. Found: C, 20.00; H, 2.33; N, 17.47. IR (KBr pellet, cm^{-1}): 424w, 510 m, 612m, 632m, 698m, 786m, 890m, 978s, 1054s, 1100s, 1158s, 1192m, 1218s, 1274s, 1300s, 1328s, 1362s, 1386s, 1496w, 1564s, 1642s, 2964m, 3004m, 3044m, 3136s, 3306m, 3460m, 3524m. At 130−140 °C, the reaction proceeded with the formation of two products: green-blue prisms **1a** and an unidentified deep-blue powder. The latter is even more stable under severe conditions (>165 °C).

*[$Cu_3(\mu_3$-OH)(trgly)$_3$(H_2O)$_3$]SO_4·16H_2O (**1b**).* **1b** was prepared by a slow interdiffusion of CH_3CN/H_2O (1:1) solutions (or ∼0.5% aqueous solution of benzonitrile) of $CuSO_4$·5H_2O and **trgly-H**. A CH_3CN/H_2O (1:1, 0.5 mL) solution was layered onto solid $CuSO_4$·5H_2O (12.5 mg, 0.050 mmol) which was placed in a narrow-diameter test tube (length/diameter size = 30 mm × 5 mm, ∼0.5 mL). The tube then was put into a larger size vial (50 mm × 20 mm, ∼12 mL) containing **trgly-H** (13.6 mg, 0.100 mmol) in CH_3CN/H_2O (1:1, ∼8 mL). For interdiffusion of the components, the small test tube was immersed into the vial followed by slow addition of CH_3CN/H_2O (1:1, ∼2 mL) using a Pasteur pipet, and then the vial was capped. The slowly dissolving reaction components were left undisturbed at rt for two weeks. The resulting blue octahedral crystals were collected and dried at rt. (Yield 7.0 mg, 41%, please see Figure S14 in SI). Anal. Calc for $C_{12}H_{51}Cu_3N_9O_{30}S$ (%): C, 14.07; H, 5.02; N, 12.31. Found: C, 14.00; H, 4.99; N, 12.00. IR (KBr pellet, cm^{-1}): 604m, 632m, 700m, 794w, 974m, 1052s, 1092s, 1218m, 1304m, 1396s, 1564s, 1630s, 3032s, 3124s, 3400s.

Analogously, compound **1b** was isolated in 49% yield from a saturated benzonitrile aqueous solution (∼0.5%) starting from **trgly-H** (81.6 mg, 0.600 mmol), $CuSO_4$·5H_2O (153.3 mg, 0.614 mmol) and using 50 and 20 mL test tubes, respectively. The phase purity of the sample was established by comparison of the observed and simulated X-ray powder diffraction patterns (see SI). Anal. Calc for $C_{12}H_{51}Cu_3N_9O_{30}S$ (%):C, 14.07; H, 5.02; N, 12.31. Found: C, 14.19; H, 5.40; N, 12.28. This method can be applied for the bulk synthesis of complex **1b**.

Our attempts aimed at optimizing postsynthetic activation procedures of compound **1b** for further gas sorption measurements, similar to those recently described by one of us,[9b] were unsuccessful due to easy structural conversion processes (Figure S24 in SI).

*$Cu_3(\mu_3$-OH)(d-trala)$_3$(ClO_4)$_{0.5}$](ClO_4)$_{1.5}$·1.5H_2O (**2**).* A mixture of $Cu(ClO_4)_2$·6H_2O (36.6 mg, 0.0988 mmol), (*d*)-**trala-H** (14.1 mg, 0.100 mmol), and 2 mL of water was placed in a Teflon-lined steel autoclave, stirred for 10 min at rt and then heated at 120 °C for 36 h. Cooling to rt during the next 60 h led to green-blue plates of the product that were collected, washed with water, and dried in air. Yield 9.6 mg (34%). Anal. Calc for $C_{15}H_{22}Cl_2Cu_3N_9O_{16.5}$ (%): C, 21.10; H, 2.60; N, 14.76. Found: C, 21.01; H, 2.50; N, 14.56. IR (KBr pellet, cm^{-1}): 625s, 665m, 725m, 845m, 880m, 990, 1090ws, 1200s, 1325m, 1525s, 1735w, 2000w, 2860m, 2915m, 2955m, 3130s, 3420m.

Under similar hydrothermal conditions, the interaction of the **trgly-H** and (*d*)-**trala-H** ligands with some other Cu(II) salts containing tetrahedral anions (SO_4^{2-}, SeO_4^{2-}, ClO_4^-, BF_4^-) afforded either polycrystalline solids (**trgly-H**: SeO_4^{2-}, ClO_4^-, BF_4^- or **trala-H**: BF_4^-) or clear-blue solutions without any precipitated product (**trala-H**: SO_4^{2-}, SeO_4^{2-}).

Measurements. IR spectra (400−4000 cm^{-1}) were collected using a Perkin-Elmer FTIR spectrometer with samples prepared as KBr pellets. ^{1}H NMR spectra were recorded on a Bruker 400 MHz spectrometer. Elemental analysis (C, H, and N) was carried out with a Vario EL-Heraeus microanalyzer. PXRD was carried out on a Stoe STADIP (Cu Kα_1) using a linear PSD detector. The temperature-dependent X-ray measurements were recorded on a Stoe STADIP with a high-temperature attachment and image-plate detector system. Thermogravimetric/differential thermal analysis (TG/DTA) was carried out on a Netzsch F1 Jupiter device (the sample was heated at a rate of 10 K min^{-1}).

X-ray Crystallography. Diffraction data were collected at 296 K on a Bruker APEXII CCD area-detector diffractometer (φ scans) (graphite-monochromated Mo Kα radiation, λ = 0.71073 Å). The data were corrected for Lorentz-polarization effects and for the effects of absorption (multiscans method). The structures were solved by direct methods and refined by full-matrix least-squares on F^2 using the SHELX-97 package.[15] For complex **1b**, contribution of all disordered water molecules was modeled using the Squeeze routine as implemented in Platon.[16]

Crystallographic data and experimental details for structural analyses are summarized in Table S1 in SI. The crystallographic material can also be obtained from the CCDC, the deposition numbers being CCDC **949597**, **949599** (for **1a** and **1b**, respectively) and **949598** (for **2**).

Magnetic Properties. Magnetic susceptibility data of powdered samples were measured on a Quantum Design SQUID magnetometer MPMSXL-5 (Faculty of Chemistry, Wroclaw University), over the temperature range 1.8−300 K at the magnetic induction of 0.5 T. Corrections for the sample holders were applied. Diamagnetic corrections were determined from Pascal's constants.[17]

EPR Spectra. High-field, high-frequency EPR spectra at temperatures ranging from ∼3 to 300 K were recorded on a home-built transmission spectrometer at the EMR facility of NHMFL.[18]

The instrument is a transmission-type device in which microwaves are generated by a phase-locked Virginia Diodes source producing harmonics of its 13 ± 1 GHz base frequency, of which the second, fourth, sixth, eighth, 16th, 24th, and 32nd were available. A superconducting magnet (Oxford Instruments) capable of reaching a field of 17 T was employed. The powder samples were not constrained and showed no magnetic torquing at high magnetic fields.

RESULTS AND DISCUSSION

1,2,4-Triazol-4-yl-acetic acid is a known compound and was synthesized by Garcia in two similar ways starting either from glycine (one-pot reaction, 50% yield)[19] or glycine ethyl ester hydrochloride (two-step reaction, ∼58% total yield),[11] whereas (*d*)-2-(1,2,4-triazol-4-yl)-propionic acid had not been described yet. In the present study we tried to follow the traditional

dx.doi.org/10.1021/ic403148f | Inorg. Chem. 2014, 53, 3642−3654

synthetic method using the corresponding amino acid (gly or (*d*)-ala; amine source) and *N*,*N*-dimethylformamide azine in boiling toluene. These reaction conditions are frequently applied for aromatic and heterocyclic amines.[14] The transamination reaction afforded a viscous dark oil and thus required extensive purification. However, a simple workup procedure, including the preparation of potassium intermediates (**trgly-K** and **trala-K**) and their further conversion to **trgly-H** and **trala-H** by treatment of **trgly-K** (or **trala-K**) with HCl in ethanolic solution, was employed. Despite the low total yield (27−30%) of the final products, this method allows preparation of triazolyl-carboxylic acids and their simple salts from suitable precursors avoiding chromatography. Moreover, the potassium salts are potentially interesting building blocks for construction of MOFs.

The reaction of 1,2,4-triazole carboxylic acids (**trgly-H**, (*d*)-**trala-H**) with Cu^{2+} salts in water at nearly neutral pH, accompanied by deprotonation of the organic ligand and simultaneous hydrolysis of the Cu^{2+} cations, proceeds efficiently under hydrothermal conditions (Scheme 2) affording the basic

Scheme 2. 1,2,4-Triazole Carboxylate Building Blocks, Derived from *α*-Amino Acids, Represent a Straightforward Pathway toward the Incorporation of Triangular [$Cu_3(\mu_3$-OH)] Clusters into MOFs

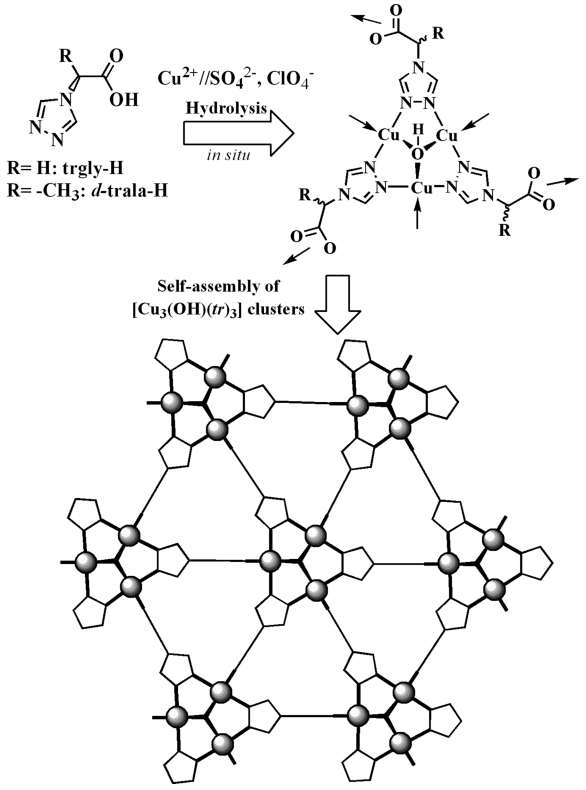

μ_3-hydroxo species (pure crystalline phases of complexes **1a** and **2**). Similar reactions carried out at room temperature led to immediate formation of blue precipitates (for **trgly-H**/Cu^{2+}:SO_4^{2-}, ClO_4^-, BF_4^-), which contained a mixture of products (including compound **1b**; please see observed and calculated XRPD patterns shown in Figure S25 in SI), or deep-blue solutions (for (*d*)-**trala-H**/Cu^{2+}:SO_4^{2-}, ClO_4^-, BF_4^-).

These triangular [$Cu_3(\mu_3$-OH)] hydroxoclusters can serve as self-associating building units; that is one of the key factors in understanding the resultant structural topologies in compounds **1a**, **1b** and **2**. First, in the [$Cu_3(\mu_3$-OH)] core each pair of Cu^{2+} cations is primarily supported by a [−N-N-] triazole fragment which can be regarded as a complementary unit to the short inorganic bridge (e.g., μ_3-OH). The carboxylate moieties connect the clusters into extended layer or zeolite-like structures.

The asymmetric unit in complex [$Cu_3(\mu_3$-OH)-(**trgly**)$_3$(SO_4)]·$2H_2O$ (**1a**, space group $P2_1/c$) contains one cluster molecule with three independent Cu atoms, each of them adopting a square-pyramidal N_2O_2 + O environment. In the basal plane the coordination arrangement is achieved by two *trans*-coordinated N(*tr*) atoms and two oxygen atoms from μ_3-OH and singly bound −O−C═O groups. The axial sites above the cluster plane are perfectly suited for cooperative interactions with tripodal μ_3-SO_4^{2-} anions (Figure 1, Table 1).

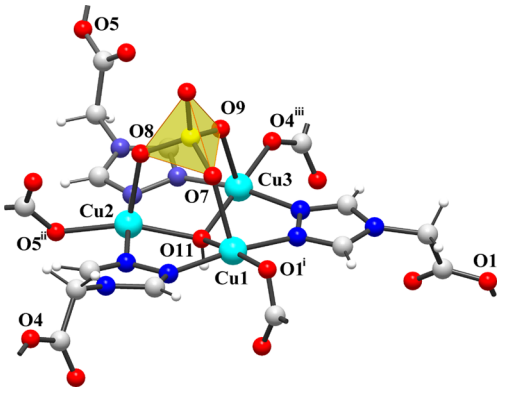

Figure 1. In the structure of **1a**, the triangular hydroxo-cluster of [$Cu_3(\mu_3$-OH)(**trgly**)$_3$] is stabilized by a facially coordinating tripodal SO_4^{2-} anion, symmetry codes: (i) *x*, −*y*+3/2, *z*−1/2; (ii) *x*, −*y*+1/2, *z*−1/2; (iii) *x*, *y*, *z*+1.

Each triangular subunit is connected to six surrounding triangles through O atoms of carboxylate groups. Considering the [$Cu_3(\mu_3$-OH)] clusters as 6-fold-connected nodes, the resultant topologic motif can be classified as a 2D uninodal uniform (3,6) coordination network. A similar subtopological type was observed earlier in the related [{$Cu_3(\mu_3$-OH)}(μ_3-*btr*)$_3$]$^{n+}$ cationic framework.[20] The small trigonal cavities of the [$Cu_3(\mu_3$-OH)(**trgly**)$_3$(SO_4)] network are occupied partially by uncoordinated water molecules and the apical O-atom of the sulfate ligand (Figure 2).

A semi-rigid methylene linkage between triazole and carboxylate groups in the **trgly** ligand dictates the angular orientation of Cu−N and Cu−O bonding vectors in the coordination network. Such ligand−metal interaction leads to wave-like layers (Figure 2) in which the cluster centers are positioned at distances of 10.542, 10.642, and 12.096 Å, whereas the closest interlayer separations between triangular centroids are significantly shorter (5.294 Å). Being stabilized by numerous hydrogen bonds (μ_3-OH···O−C═O 2.806 Å, HO−$H_{(aqua)}$···OSO_3 2.777 Å), the two closest neighboring sheets are tightly stacked in a ABAB manner that unexpectedly results in the disposition of sulfate anions on only one side of the layers.

The self-assembly of the enantiopure ligand, (*d*)-**trala**, and $Cu(ClO_4)_2$ under hydrothermal conditions affords the coordination network of [$Cu_3(\mu_3$-OH)(*d*-**trala**)$_3$(ClO_4)$_{0.5}$]-(ClO_4)$_{1.5}$·$1.5H_2O$ (**2**) crystallizing in the non-centrosymmetric space group $R3_2$. At first glance, the local shape and geometry

dx.doi.org/10.1021/ic403148f | Inorg. Chem. 2014, 53, 3642−3654

Table 1. Selected Bond Lengths (Å) in Compounds 1a, 1b and 2

bond type	$[Cu_3(\mu_3\text{-}OH)(\mathbf{trgly})_3\ (SO_4)]\cdot 2H_2O$, (**1a**)	$[Cu_3(\mu_3\text{-}OH)(\mathbf{trgly})_3\ (H_2O)_3]SO_4\cdot 16H_2O$, (**1b**)	$[Cu_3(\mu_3\text{-}OH)(d\text{-}\mathbf{trala})_3(ClO_4)_{0.5}]\ (ClO_4)_{1.5}\cdot 1.5H_2O$, (**2**)
Cu−N(*tr*) (eq. plane)	1.976(3)−1.987(3)	1.967(4)	1.992(3), 2.001(3)
Cu−O(H) (eq. plane)	2.027(2)−2.030(2)	2.009(3)	2.0337(13)
Cu−O(C═O) (eq. plane)	1.926(3)−2.004(3)	1.967(4)	1.954(3)
Cu−O(C)− (axial)	–	–	2.359(4)
Cu−$O_{(anion)}$ (axial)	2.174(3)−2.190(3)	–	2.519(15)
Cu−Oaqua (axial)	–	2.241(7)	–
Cu···Cu distance within $[Cu_3(\mu_3\text{-}OH)]$	3.3562(6)−3.3804(6)	3.3950(15)	3.4447(9)
closest intercluster Cu···Cu distance	3.499	8.512	4.433

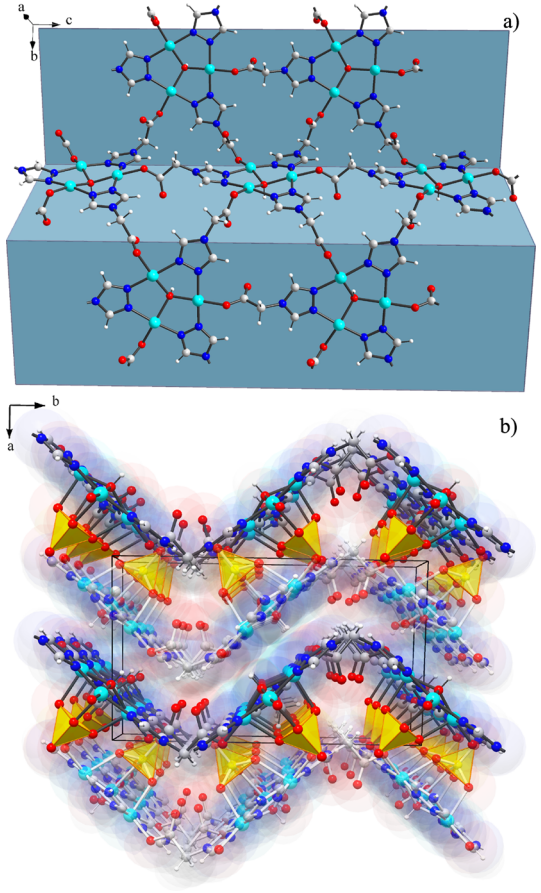

Figure 2. (a) Two-dimensional wave-like layer in **1a** having uninodal uniform (3,6) topology; (b) layered packing showing the ABAB stacking mode.

of the building block $[Cu_3(\mu_3\text{-}OH)(\mu_2\text{-}tr)_3]$ remains unchanged in comparison to those of complex **1a**. However, in contrast to those of **1a**, the Cu ions are in a pseudo-octahedral coordination environment $[N_2O_2 + 2O]$, in equatorial plane defined by two triazole N atoms (N1, N2), an oxygen atom of a carboxylate moiety (O3), and the inorganic bridge μ_3-OH (O1). The axial positions on one face of the C_{3v} symmetric copper cluster are occupied by O-atoms of μ_3-ClO_4^-, whereas the opposite side is completed by oxygen atom (O2) of another carboxylate function (Figure 3, Table 1). Such discrimination toward axially bound ligands results in the specific location of the methyl groups sitting above the $[Cu_3(\mu_3\text{-}OH)]$ plane.

Presumably because of its more basic character, the deprotonated **trala** ligand exhibits a tetradentate coordination

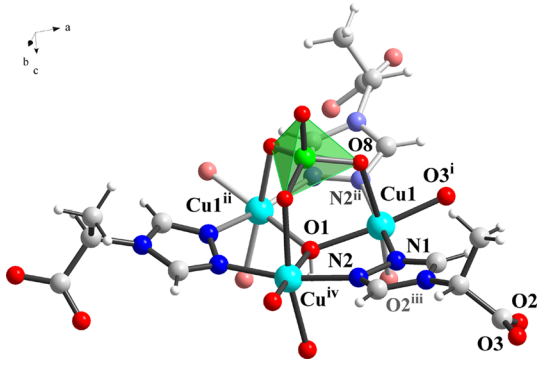

Figure 3. Perchlorate-capped equilateral triangular hydroxo-cluster $[Cu_3(\mu_3\text{-}OH)((d)\text{-}\mathbf{trala})_3]$ in complex **2** has a cone-shaped geometry. Symmetry codes: (i) $-y+1, x-y, z$; (ii) $-x+y,-x, z$; (iii) $y-1/3, x-2/3, -z+4/3$; (iv) $-y, x-y, z$.

mode that increases the structural integrity of clusters in the polymer network. In **2**, the 2D topological motif reminds us of a combination of two equivalent uninodal (3,6) nets shifted in the ab plane (Figure 4). μ_2-Carboxylate groups efficiently interlink two $[Cu_3(\mu_3\text{-}OH)]$ units from the upper and lower sheet, keeping them at a Cu···Cu distance of 4.433 Å. In the

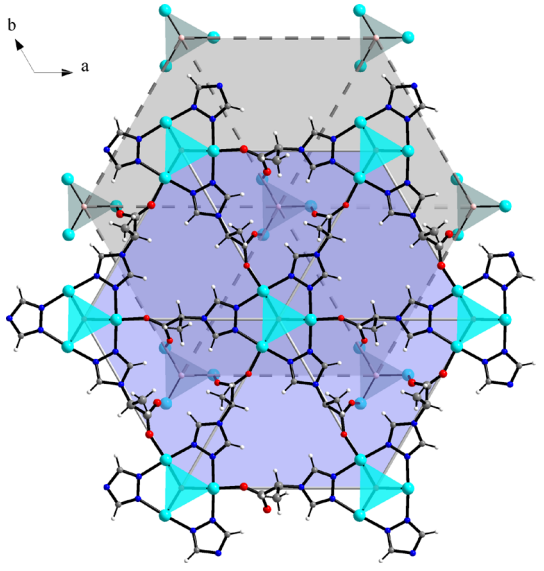

Figure 4. In the structure of $[Cu_3(\mu_3\text{-}OH)((d)\text{-}\mathbf{trala})_3(ClO_4)_{0.5}]\text{-}(ClO_4)_{1.5}\cdot 1.5H_2O$ (**2**), the formation of a double-layer motif through μ_2-carboxylate interlinks between two identical (3,6) coordination layers led to a novel topological type (two-nodal 3,9-c net).

dx.doi.org/10.1021/ic403148f | Inorg. Chem. 2014, 53, 3642−3654

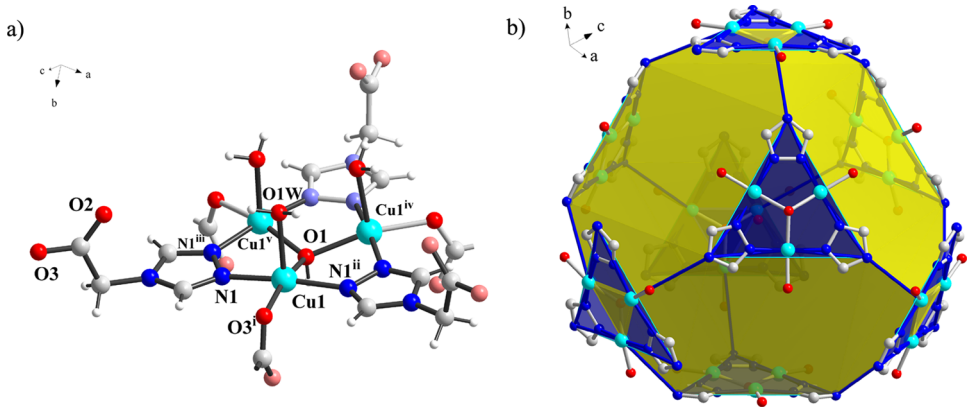

Figure 5. (a) The equilateral triangular $[Cu_3(\mu_3\text{-OH})(\mathbf{trgly})_3(H_2O)_3]$ cluster in complex **1b**, (b) the construction of an Archimedean polyhedron, a truncated cube, via self-assembly of eight $Cu_3(\mu_3\text{-OH})$ triangles using a "symmetry-interaction approach". Symmetry codes: (i) $-z+1/2, x+1/2, -y+1/2$; (ii) z, y, x; (iii) x, z, y; (iv) y, z, x; (v) z, x, y.

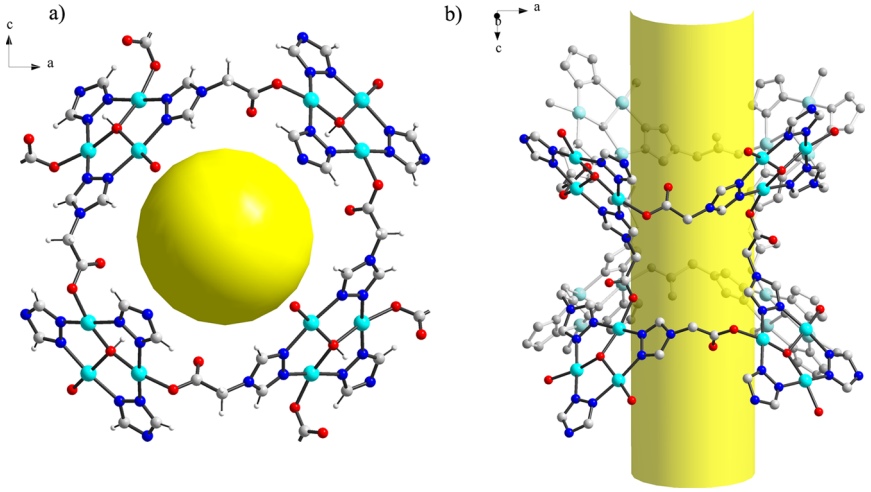

Figure 6. Fragments of the crystal structure of **1b** showing the formation of cages and open channels.

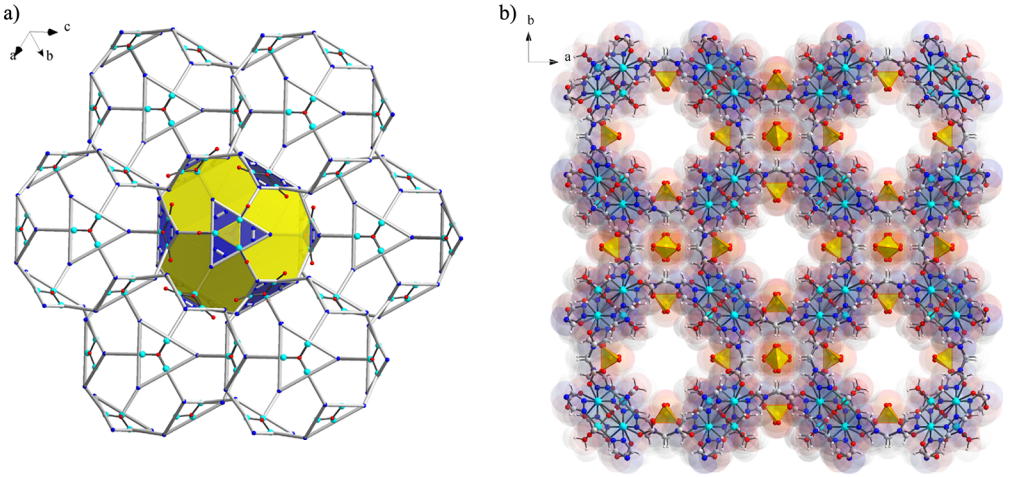

Figure 7. (a) Crystal packing of the pseudo-truncated cubes which are connected via common triangular faces. (b) Two kinds of channels (2 × 2 and 10 × 10 Å) run along the crystallographic axes. Uncoordinated SO_4^{2-} anions (shown as tetrahedra) and water molecules are lodged within the channels.

resulting double layer, each equilateral triangular cluster serves as 9-fold-connected node, whereas the organic ligand acts as 3-fold-connected one. Thus, the net belongs to a novel two-nodal 3,9-c topology with Schläfli point symbol $\{4^{18}.6^{18}\}\{4^2.6\}_3$.[21]

In **2**, the cationic $[Cu_3(\mu_3\text{-OH})((d)\text{-}\mathbf{trala})_3(ClO_4)_{0.5}]_n$ layers require additional counteranions to maintain the overall charge-balance. The required uncoordinated ClO_4^- anions are readily accommodated between the double-layer motifs.

dx.doi.org/10.1021/ic403148f | Inorg. Chem. 2014, 53, 3642−3654

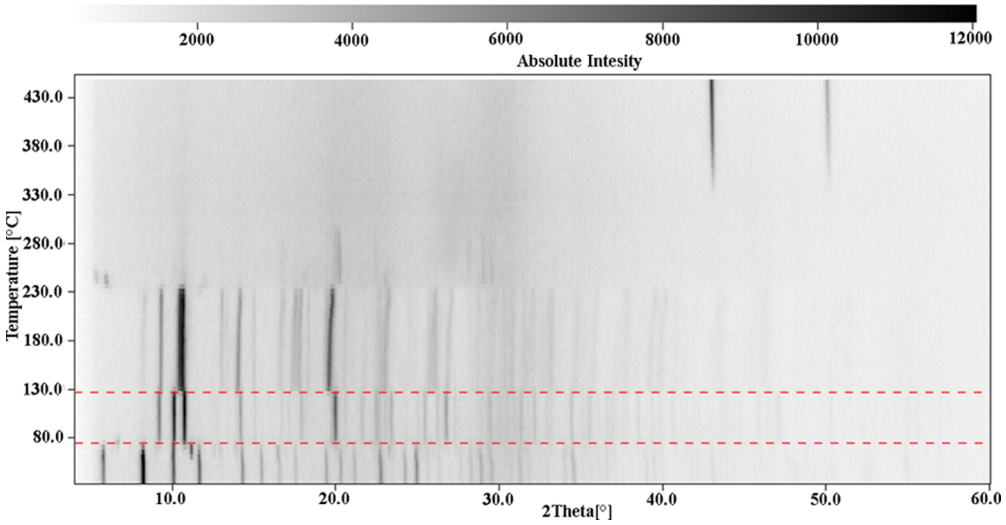

Figure 8. Thermo-PXRD pattern (2θ = 5−60°) for complex **1b** shows a double-step thermal conversion (at 60−70° and at 120−130 °C, red dashed lines) which is accompanied by visible color changes from blue to green and then deep blue.

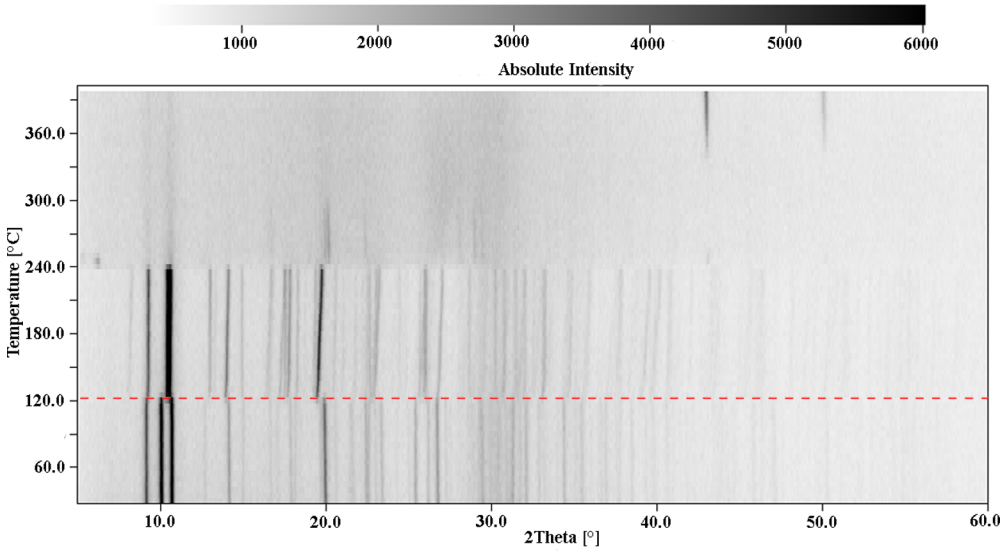

Figure 9. The Guinier−Simon diagram (2θ = 5−60°) of complex **1a** shows a single-step transformation at ∼120−130 °C (red dash line) that leads to an unknown crystalline phase. Similar transformations are observed for compound **2** (Figure S23 in SI).

The interaction of $CuSO_4$ with **trgly-H** proceeding at room temperature demonstrates another challenging alternative of the mixed donor triazole-carboxylate systems in the design of microporous zeolite-like frameworks consisting of $Cu_3(\mu_3\text{-OH})$ SBUs (secondary building blocks). In the 3D network of $[Cu_3(\mu_3\text{-OH})(\mathbf{trgly})_3(H_2O)_3]SO_4{\cdot}16H_2O$ (**1b**) with cubic symmetry (space group $I\bar{4}3m$), the organic ligand, similarly as in complex **1a**, acts as a tridentate module with well-defined coordination functions of *tr* and $-COO^-$. The coordination environment around each copper ion is square-pyramidal $[N_2O_2{+}O]$, but unlike the tripodal binding mode of sulfate in **1a**; here the one-side axial positions are occupied only by aqua ligands with a distant contact Cu−O of 2.241(7) Å (Figure 5a). Three carboxylate fragments around the C_{3v} symmetric $[Cu_3(\mu_3\text{-OH})(tr)_3]$ core are arranged above or below the cluster plane. This donor direction of the $-COO^-$ groups is perfectly suited to form spherical polyhedra or cage-like assemblies according to the so-called 'directional-bonding' concept.[22] All $Cu_3(\mu_3\text{-OH})$ clusters as 6-fold-connected nodes are further assembled in a cubic array possessing α-Po topology (pcu: $4^{12}.6^3$). The structural motif is identical to $[Cu_3(\mu_3\text{-O})(\mathbf{trgly})_3(H_2O)_3]BF_4{\cdot}H_2O$ described in ref 11. As a matter of fact, compound **1b** should be classified as an Archimedean solid.[23]

The unit cell of **1b** contains eight trinuclear clusters that form a convex polyhedron, a giant truncated cube, constructed from two kinds of faces: eight triangles of two types and six irregular octagons. The diagonal distance between opposite triangle centroids is 18.305 Å (Figure 5). The neighboring polyhedra are condensed through the common triangular faces yielding two sets of parallel channels, with van der Waals cross sections of 2 × 2 and 10 × 10 Å, where guest water molecules and SO_4^{2-} anions reside (Figures 6, 7). Similarly to BF_4^- anions in $[Cu_3(\mu_3\text{-O})(\mathbf{trgly})_3(H_2O)_3]BF_4{\cdot}H_2O$,[11] either SO_4-tetrahedra becomes encapsulated in the small cavity that supported by two kinds of H-bonding contacts. One belongs to a bifurcated type between *tr*-fragments (C_{tr}−H) and O-$(SO_3)^{2-}$, while the other

dx.doi.org/10.1021/ic403148f | *Inorg. Chem.* 2014, 53, 3642−3654

arises from uncoordinated water molecules (in SI see Table S6 and Figures S7 and S8).

The solvent-accessible volume, after removing the bound and unbound water molecules, is calculated (PLATON program) to be 5313.5 Å^3 (or 56% of the unit cell), slightly more than for the [$Cu_3(\mu_3$-O)] tetrafluoroborate analogue.[11] Interestingly, the similar microporous framework crystallizing in the same space group was achieved for [$Cu_3(\mu_3$-O)] clusters with angular 3-(1,2,4-triazol-4-yl)-pyridine ligands and tetrahedral counter-anions (BF_4^- and ClO_4^-).[24] This may indicate that the construction of the cage-like motifs is accomplished by directional bonding being preprogrammed in the ligand functionality and angular geometry.

Thermal Transformations. The thermal behaviors of complexes **1a** and **1b** were studied using temperature-dependent powder X-ray diffractometry (TD PXRD). The results clearly demonstrate the occurrence of interesting structural phase transitions. As shown in Figure 8, in the temperature interval from 20 to 230 °C the microporous framework **1b** undergoes a two-step structural transformation before the sample loses its crystallinity. The first conversion in the range of 60−70 °C afforded exclusive formation of the two-dimensional network **1a**, as evidenced by comparison of the experimental and simulated powder patterns. This phase is sufficiently stable up to ∼130 °C, while a further gradual heating leads to sharp changes in the PXRD pattern yielding a new but, unfortunately, unidentified crystalline phase, which remains intact up to 230 °C. The observations are correlated with the Guinier−Simon diagram of complex **1a** (Figure 9) which shows just one thermal phase transformation at 120−130 °C. As indicated in the TGA experiments (see SI), the structural changes are accompanied by the gradual release of water molecules in the temperature ranges of 60−200 °C (for complex **1a**) and 30−240 °C (for **1b**). However, these DTA data are not very informative because the dehydration processes do not proceed in a stepwise manner, synchronously with the structural transformations.

Interestingly, when the synthesis of compound **1a** (see Experimental Section) was carried out at 130−140 °C, a mixture of two products (green prisms **1a** and deep-blue powder of the unknown phase) were formed in close proportions. The deep-blue phase is only a product when the hydrothermal process temperature was set at 165 °C. Obviously, the thermal behavior suggests that the microporous [$Cu_3(\mu_3$-OH)(**trgly**)$_3$(H_2O)$_3$]SO_4·16H_2O framework with the 3D zeolite-like topology can be regarded as a "kinetic" product or a metastable phase. For instance, upon standing in water for over a few months the compound irreversibly transform into the denser and more stable 2D crystal structure of **1a**, *i.g.*, thermodynamic product.

Magnetic Properties and EPR Spectra. In the trimeric units of both compounds **1a** and **1b** the three copper ions arranged in a triangle are bridged by triazole molecules and by the O atom of OH−. The groups bridging different trinuclear units to each other contain a tetrahedral carbon atom and thus are unlikely to transmit significant exchange interactions. From the viewpoint of magnetism, the trinuclear units can thus be treated separately. The magnetic moment of **1a** (per three copper(II) ions) is indicative of strong antiferromagnetic interactions. The isotropic exchange interactions in a trinuclear system can be analyzed by using the Heisenberg−Dirac−Van Vleck Hamiltonian:[7]

$$\hat{H}_{HDVV} = J_{12}\hat{\mathbf{S}}_1\hat{\mathbf{S}}_2 + J_{13}\hat{\mathbf{S}}_1\hat{\mathbf{S}}_3 + J_{23}\hat{\mathbf{S}}_2\hat{\mathbf{S}}_3 \quad (1)$$

In this notation, the J values are positive for antiferromagnetic interactions. Three states of the total spin operator of the system, $\hat{\mathbf{S}}_T = \hat{\mathbf{S}}_1 + \hat{\mathbf{S}}_2 + \hat{\mathbf{S}}_3$, are possible: one quartet state with the quantum number $S_T = 3/2$ and two doublet states with $S_T = 1/2$. If $J_{12} = J_{13} = J_{23} = J$, then the quartet state lies 3/2 J above the degenerate pair of the doublet states. In a situation where $J_{12} = J_{23} = J_1 \neq J_{13} = J_2$, the doublet states split, and the energies of the quartet state (Q) and of the two doublet states (D1 and D2) are:[7,25]

$$E_Q = J_1/2 + J_2/4$$
$$E_{D1} = -J_1 + J_2/4$$
$$E_{D2} = -3J_2/4 \quad (2)$$

as shown in Figure 10.

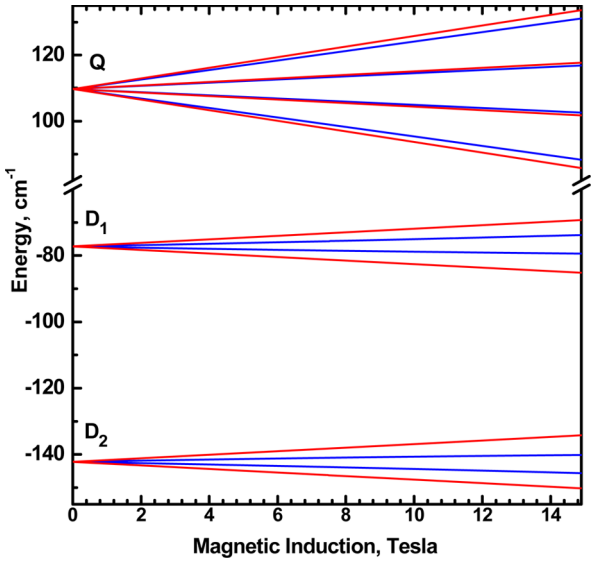

Figure 10. Energy levels of a trinuclear Cu(II) system according to Hamiltonian (eq 3), calculated with $g_x = g_y = 2.07$, $g_z = 2.33$, $J_1 = 138$ cm^{-1}, $J_2 = 163$ cm^{-1}. The G_z components of all antisymmetric interactions 1−2, 1−3, and 2−3 are equal to 35 cm^{-1}. Labels Q, D1, and D2 indicate the quartet and two doublet states (see Formula 2).The red and blue lines were calculated for the magnetic field perpendicular (orientation Z) and parallel to the Cu3 plane (X,Y), respectively. It is seen that the Zeeman splitting in the doublet states D1 and D2 is reduced at the X,Y orientation as a result of the antisymmetric exchange interactions. When $J_1 = J_2$ and $G_z \neq 0$, that splitting vanishes.

At sufficiently low temperatures, only the D2 doublet is populated, and the magnitude of the magnetic moment referred to the entire trinuclear entity at low temperatures should be $\mu = g\sqrt{3/4}$ where g is the average g value, typically about 2.1 for Cu^{2+}. This results in μ_{eff} of some 1.8 μ_B, or χT = 0.4 cm^3 mol^{-1} K, corresponding to one unpaired electron per three copper ions. The experimental χT magnitudes in Figure 11 are much smaller than this (∼0.2 cm^3 mol^{-1}K) which cannot be explained on the basis of Hamiltonian (eq 1) only. Two interesting phenomena must be taken into account when dealing with the antiferromagnetic triangular systems. One is the 'spin frustration' which is the impossibility of orienting each pair of spins in the antiparallel fashion at the same time. The

dx.doi.org/10.1021/ic403148f | Inorg. Chem. 2014, 53, 3642−3654

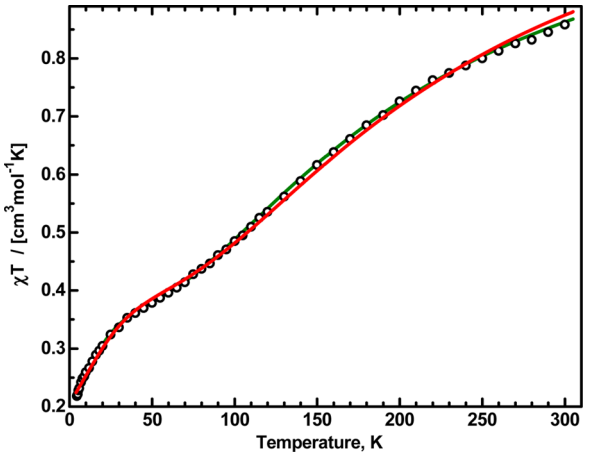

Figure 11. The temperature dependence of the product χT for **1a**. Circles: experimental; red solid line: calculated using spin Hamiltonian 3 with $g_x = g_y = 2.07$, $g_z = 2.33$, $J_1 = 138$ cm^{-1}, $J_2 = 163$ cm^{-1}. The z components of the antisymmetric interactions 1−2 and 2−3 (G_{z1}) as well as 1−3 (G_{z2}) are equal to 34 cm^{-1}. These data can be fitted substantially better when the g parameters are allowed to vary, but then g_z is obtained unacceptably low ($g_{x,y} = 2.05$, $g_z = 2.07$, $J_1 = 119$ cm^{-1}, $J_2 = 143$ cm^{-1}, $G_{z1} = 25$ cm^{-1}, $G_{z2} = 25$ cm^{-1}), green line. The green and red lines overlap below ~80 K.

second is the antisymmetric exchange interaction, also called the Dzialoshinskii−Moriya term. The DM interaction between atoms "i" and "j" is represented by a dot-product of a vector quantity G_{ij} with the cross-product of the spin operators $\hat{S}_i$ and $\hat{S}_j$: $G_{ij}\cdot\hat{S}_i \times \hat{S}_j$. There are three such DM terms in the full spin Hamiltonian for a triangular trimer:

$$\hat{\mathbf{H}} = \mu_B \vec{B} \sum_i \{g\}_i \hat{S}_i + \sum_{i<j} \sum_j \hat{S}_i \{J\}_{ij} \hat{S}_j + \sum_{i<j} \sum_j \vec{G}_{ij}\cdot\hat{S}_i \times \hat{S}_j \quad (3)$$

The indices i, j number the atoms in the trimer. The symmetric $\{\mathbf{J}\}_{ij}$ tensors describing interactions in a pair i,j may be anisotropic and thus may contain the zero-field splitting effects. The scalar parameters J_{12} etc. in eq 1 equal one-third of the trace of a respective tensor, like $J_{12} = (\{J_{xx}\}_{12} + \{J_{yy}\}_{12} + \{J_{zz}\}_{12})/3$. Each of the $\mathbf{G}_{ij}$ vectors (for a pair i−j) in our system is expected to have their largest component G_{zij} perpendicular to the plane of the three copper ions.[7] This direction is also very close to the expected direction of the g_z component for each copper. The second largest components, if present, will lie in the $Cu_1Cu_2Cu_3$ plane and be perpendicular to the Cu−Cu vector of a pair. The components along the Cu−Cu direction are expected to be close to zero and are assumed to be zero. Further in this paper we will attempt to interpret the experimental data, assuming that all three copper ions have the same values of g_z, g_x and g_y. Both the isotropic and antisymmetric parts of the interactions 1−2 and 2−3 are assumed to be equal, while the interaction 1−3 may be different from them. We will thus use $J_1 = J_{12} = J_{23}$ and $J_2 = J_{13}$, as in eq 2 and $\boldsymbol{G}_1 = \boldsymbol{G}_{12} = \boldsymbol{G}_{23}$, $\boldsymbol{G}_2 = \boldsymbol{G}_{13}$. The components of the $\boldsymbol{G}_1$ and $\boldsymbol{G}_2$ vectors will be named G_{1x} etc.

The theory of the antisymmetric exchange can be found in many sources.[7a,26,27] Here we would like to emphasize that this interaction disappears when the interacting ions are related by an inversion center. The components of the $\mathbf{G}_{ij}$ vectors are of the order of $(\Delta g/g)\cdot J_{gigj}^{eigj}$ where Δg is the deviation of the g value in a complex from 2.0023 and the symbol J_{gigj}^{eigj} refers to exchange interaction in a pair "i,j" of copper atoms of which atom "j" is in its ground state (g) and the other one is in an excited state (e).[7] These g deviations are large in Cu(II): a value of g_z of 2.30 was found in a linear trinuclear complex with 1,3-bis(1,2,4-triazol-4-yl)adamantane,[25] and accordingly, the antisymmetric exchange may contribute significantly to the properties of a triangular system. The most interesting consequence is quenching of the effective g values in the doublet states of a triangular system. This quenching, occurring when the magnetic field lies in the triangle plane affects both the EPR spectra and the magnetic susceptibility.

A program was written by one of us to fit both the magnetic susceptibility and EPR data on the basis of the Hamiltonian eq 3. The program performed numerical diagonalization of the 8 × 8 spin Hamiltonian matrix to evaluate the energy levels. The magnetic susceptibility at the magnetic field B and an orientation given by the polar angles Θ, Φ was calculated from

$$\chi(\Theta, \Phi) = -\frac{N}{B}\frac{\sum_{i=1}^{8} \frac{\partial E_i(\Theta,\Phi)}{\partial B} \exp(-E_i(\Theta, \Phi)/kT)}{\sum_{i=1}^{8} \exp(-E_i(\Theta, \Phi)/kT)} \quad (4)$$

where the derivatives $\delta E_i/\delta B$ were calculated numerically by evaluating the energies E_i 5 G below and 5 G above the working magnetic field of the SQUID magnetometer (5000 G). The powder susceptibility was then calculated in a manner similar to the way by which the powder EPR spectra are simulated, that is, it was numerically integrated with $\sin\Theta d\Theta d\Phi$. The fit results for **1a** are presented in Figure 11. The spin Hamiltonian parameters $g_x = g_y = 2.07$, $g_z = 2.33$, $J_1 = 138$ cm^{-1}, $J_2 = 163$ cm^{-1}, $\mathbf{G}_{z1} = \mathbf{G}_{z2} = 34$ cm^{-1} were found. Since the magnetic data for out three compounds are difficult to present in one figure, data for **2** and **1b** are given in the SI, Figure S26. The spin Hamiltonian parameters for **2** are $g_x = g_y = 2.07$, $g_z = 2.33$, $J_1 = 154$ cm^{-1}, $J_2 = 193$ cm^{-1}, $G_{z1} = 38$ cm^{-1}, $G_{z2} = 39$ cm^{-1}. Problems were encountered in the case of **1b**, whose porosity and high water contents cause uncertainty in the molar mass at the time of the magnetic measurement. Chemical analysis of a sample performed just after the magnetic susceptibility measurement indicated a formula $[Cu_3(\mu_3\text{-}OH)(trgly)_3(H_2O)_3]SO_4\cdot 22H_2O$ instead of $[Cu_3(\mu_3\text{-}OH)(trgly)_3(H_2O)_3]SO_4\cdot 16H_2O$ from X-ray and earlier chemical analyses. The magnetic fitting was still less successful than for **1a** or **2**, resulting in parameters which are not reasonable (see Figure S26 in SI).

EPR Simulations. Upon finding a resonance field by an iterative procedure, the eigenvectors ψ_i and ψ_j of the levels involved in a transition were evaluated, and relative transition probability was calculated. The intensity of a transition was taken as a product of the probability and the population difference between the levels ψ_i and ψ_j obtained from the Boltzmann distribution. That procedure was repeated thousands of times for various orientations of the steady magnetic field B to generate a powder EPR spectrum.

In **1a**, the normal to the least-squares planes N_2O_2 of the equatorial ligands of each copper ion form angles 7.1°, 7.4°, and 3.0° with the respective Cu−$O_{sulfate}$ vectors. This is a good case of an elongated square-pyramid and there is no doubt that the ground state of the copper ions is $d_{x^2-y^2}$. The direction of the largest g component, g_z, of each ion is expected to be perpendicular to its equatorial ligands plane, and it was so assumed in the following calculations. However, the smaller g_x and g_y components are likely not to be equal to each other because of the mixed N, O coordination in the equatorial plane.

dx.doi.org/10.1021/ic403148f | Inorg. Chem. 2014, 53, 3642−3654

The distances in two copper pairs in the triangle are 3.380, 3.374, and 3.356 Å, respectively, and the $Cu_1Cu_2Cu_3$ triangle is approximately isosceles. The vector perpendicular to the $Cu_1Cu_2Cu_3$ plane was taken as the Z axis of the trinuclear entity. The g_z directions of the three copper ions deviate from Z by 13.3°, 6.8°, and 14.4°, respectively. The symmetry of **1b** is higher yet, as the molecule has C_{3v} symmetry with the hydroxyl oxygen atom lying on the three-fold axis. The deviation between the normal to the least-squares plane N_2O_2 and the $Cu-O_{water}$ vector is 1.7° for each metal ion. The $Cu_1Cu_2Cu_3$ triangle is equilateral, and the Z axis of the trinuclear entity, defined as above, deviates by just 4.0° from each of the $Cu-O_{water}$ vectors.

The high-field EPR spectra of both species **1a** and **1b** were very weak because of enormous width of the resonance lines (1 T for resonance D in Figure 12) and noisy, yet they were well

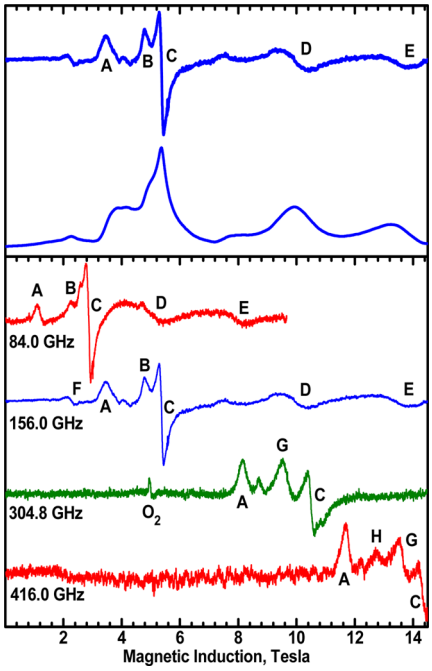

Figure 12. (Top) EPR spectrum of **1a** recorded at 3 K with ν = 156.0 GHz (upper trace) also showing the integrated spectrum (lower trace). (Bottom) Spectra recorded at 3 K with microwave frequencies as indicated. Note that the resonances *D* and *E* travel about a double distance compared to resonances *A*, *B*, and *C* when the frequency is changed from 84 to 156 GHz. Resonance labeled O_2 is due to oxygen, and it is often observed in the high-frequency EPR at or below 30 K.

reproducible. Figure 12 shows high-frequency EPR spectra of **1a** recorded at 3 K with various microwave frequencies. The prominent resonance lines which could be followed over a wide microwave frequency range are marked with letters A–H. Figure 13 shows the frequency dependence of those lines. The X-Band EPR spectra (~9.5 GHz) of **1a** were very poorly resolved showing a narrower transition at the effective g value of 2.08 (corresponding to C) and very broad transitions at g_{eff} of 1.38 and 0.75. No features similar to those reported in ref 7a for closely related complexes could be observed in X-Band. No transitions at low g_{eff} were seen in the EPR spectra of **2** and **1b**. The HF EPR spectra of **1a**, like those in Figure 12 could be only observed at the temperatures lower than 30 K. At higher temperatures the resolution decreased, and only a transition at effective g of 2.29 was observed. No excited quartet state was

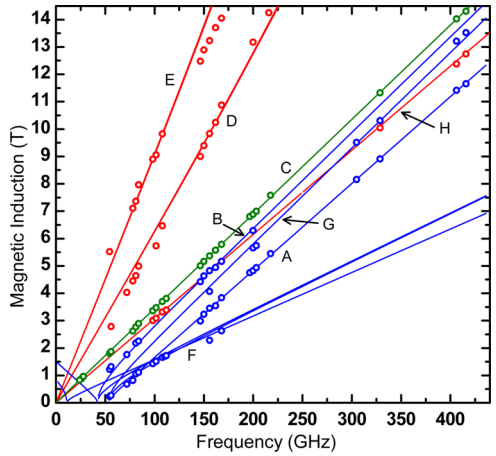

Figure 13. Frequency dependencies of the prominent resonances for **1a** shown in Figure 12. The red circles represent resonances assigned to the trinuclear species, and the red solid lines *E* and *H* were calculated by using spin Hamiltonian 3 with $g_{x,y}$ = 2.07, g_z = 2.33, J_1 = 138, J_2 = 163 cm^{-1}, $\mathbf{G}_{z1} = \mathbf{G}_{z2}$ = 34 cm^{-1}. Line *D* was calculated with $g_{x,y}$ = 2.07, g_z = 2.33, J_1 = 135, J_2 = 171 cm^{-1}, $\mathbf{G}_{z1} = \mathbf{G}_{z2}$ = 34 cm^{-1}. Blue circles and solid lines refer to the hypothetical dinuclear species. Its parameters, pertinent to the standard triplet-state spin Hamiltonian are $g_{x,y}$ = 2.05, g_z = 2.25, D = 1.6 cm^{-1}, E = 0.19 cm^{-1}. The green line C appears to be due to a mononuclear impurity with $g_{x,y}$ = 2.07. The Z component of that spectrum may overlap with line *H* (g = 2.33). The slope of these lines allows estimation of the effective g values associated with respective transitions. The g_{eff} values of 2.22, 2.13, 2.06, 1.00, and 0.91 were obtained for the branches *A*, *B*, *C*, *D*, and *E*, respectively.

seen at any conditions. When analyzing the HF EPR spectra of **1a** at 3 K (Figure 12), one has to bear in mind that only the ground state doublet is populated, which should produce at most three features in its powder spectrum, corresponding to the effective g_x, g_y and g_z values of the coupled system. The high number of resonances present must thus be explained first. Resonance "A" in Figures 12 and 13 could be followed down to the microwave frequency of ~50 GHz, at which point its position has approached zero magnetic field. The resonance therefore occurs between two levels which are split in zero magnetic field by ~1.6 cm^{-1}, and it cannot be due to a transition within a doublet spin state. The quartet state is depopulated at 3 K, and one could be tempted to assume that this branch represents a transition between the doublets D_1 and D_2 (see Figure 10). Such a small difference between the doublets cannot be reconciled with the magnetic data, however. A possible explanation could be that at some locations in the extended layers copper ions may be missing, leading to local dinuclear systems. Problems of this kind appear to be present also in ref 7a where too many resonances were observed, including transitions at zero magnetic field (in X-Band EPR) in similar triangular systems. Some of the branches in Figure 13 (blue lines and circles), including "A" can be simulated using the standard spin Hamiltonian for S = 1

$$\hat{\mathbf{H}} = \mu_B B\{g\}\hat{\mathbf{S}} + D\{\hat{\mathbf{S}}_z^2 - S(S+1)/3\} + E(\hat{\mathbf{S}}_x^2 - \hat{\mathbf{S}}_y^2) \quad (5)$$

with $g_{x,y}$ = 2.07, g_z = 2.25, D = 1.6 cm^{-1}, E = 0.19 cm^{-1}. Branch C in Figure 13 passes through the origin, and its slope indicates a g_{eff} value of 2.07. It must be assigned as the g_x branch of a mononuclear species whose g_z feature may overlap with the branch H which also passes through the origin and its g_{eff}

dx.doi.org/10.1021/ic403148f | Inorg. Chem. 2014, 53, 3642–3654

calculated from the slope is 2.33. Branch **H** is assigned to g_z of the trinuclear (and possibly also a mononuclear) species. When the microwave frequency is changed, two branches, *D* and *E*, shift much faster in magnetic field than all other resonances do. They represent the 'perpendicular' transitions in a spin-frustrated system, characterized by very low $g_{effective}$ values. The question now arises, whether they can be due to one trinuclear system—that is whether one could be an *X* and another a *Y* transition. Calculations indicate that it is not possible to find parameters which would result in the anisotropy in the CuCuCu plane sufficient for the observed behavior of the *D* and *E* features, even if nonzero *x* and *y* components of the $\mathbf{G}_1$ and $\mathbf{G}_2$ vectors are allowed. The g_x, g_y anisotropy of the three copper ions can only contribute to the width of resonances *D* and *E*, but cannot explain the large splitting between them. We are thus forced to conclude that the compound is not uniform, as similarly observed in ref 7a, and resonances *D* and *E* belong to different trinuclear entities. The parameters required to reproduce the *E* branch differ only slightly from those reproducing the *D* branch—the difference between J_1 and J_2 needs to be slightly increased, from 25 to 36 cm^{-1} while keeping $2J_1+J_2$ constant (Figure 13 caption). This sensitivity of the effective *g* to parameters may also explain the enormous line width of the *D* and *E* resonances.

In **2**, there appear to be signals at very low g_{eff} but they are yet much broader than those in **1a** and are barely distinguishable from the background (Figure S27 in SI). This may be caused by wider distribution of J_1 and J_2 in complex **2** than in **1a**, resulting in wider distribution of the g_{eff} in the former. In **1b** no such signals could be detected, and its EPR spectrum must be attributed to defects only.

Surprisingly, the more symmetric compound **1b** did not show EPR spectra similar to those of **1a**. The only resonances observed were of low intensity at $g = 2.07$ and 2.33 (Figures S28 in SI) plus a signal of "forbidden" character appearing at frequencies 200 GHz and above.

DFT Calculations. Broken symmetry calculations have been performed for both triangular systems in order to estimate the exchange integral values. The X-ray coordinates were used, but the trinuclear entity of each complex was cut out of the extended lattice by breaking the C−C bonds between the acetic acid fragments and triazoles and putting hydrogen atoms at appropriate distances from a C atom along the broken bonds. This resulted for **1a** in a neutral molecule shown in Figure 14. The same procedure produced a dipositive cation for **1b**.

The free software package ORCA was employed.[28,29] The "broken symmetry" method is designed to deal with dinuclear systems. A trinuclear case may be handled in two ways by ORCA. One possibility is to replace one of the copper atoms in the structure by Zn and calculate *J* in the system of two copper ions. Another way is to use the "spin flip" operation of ORCA on one of the copper ions. The software first performs a SCF calculation for the high-spin $S = 3/2$ state, then 'flips' the spin on one copper atom to generate the 'broken-symmetry' state with $M_S = 1/2$, performs another SCF calculation for that state, and finally uses the two energies found above to calculate the exchange integral. The calculation utilized Ahlrichs-type basis set TZVPP[30a] for Cu, S and all coordinated atoms, while SVP[30] functions were used for the remaining atoms. B3LYP[31] functional was employed. Ahlrichs polarization functions from basis H - Kr R and auxiliary bases from the TurboMole library were also used.[30b] The exchange integral value reported by ORCA must be multiplied by −2 because of the form of Hamiltonian (eq 1) used in this paper. The two methods gave comparable results. For **1a**, $J = 88$ and 100 cm^{-1} were obtained from the "zinc substitution" and spin flip method, respectively. The analogous numbers for **1b** were 106 and 136 cm^{-1}.

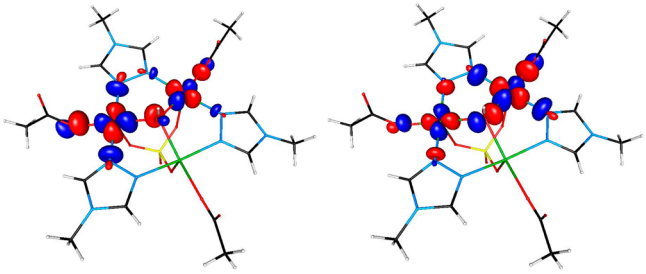

Figure 14. The symmetric (left, lower energy) and antisymmetric (right, higher energy) single-occupied molecular orbitals (SOMO) of the two-copper system in the simplified molecule of **1a** (the third copper atom was replaced by Zn).

CONCLUSION

To summarize, the mixed donor triazolyl-carboxylates (**trgly-H**, **trala-H**) derived from natural α-amino acids were explored in the design of MOFs incorporating $[Cu_3(\mu_3\text{-}OH)]$ clusters. The generation of well-defined triangular motifs exhibiting three-fold symmetry can be considered as a consequence of a synergistic ligand combination (short inorganic μ_3-OH^-, μ_3-SO_4^{2-}/ClO_4^- as well as three [−N−N−] organic bridges) and Cu^{2+} cations undergoing partial hydrolysis in aqueous media. The trimers self-associate in 2D layered (**1a**, **2**) and 3D zeolite-like (**1b**) structures. The porous zeolite-like framework (**1b**) easily transforms to 2D motif **1a** under simple heating. Further exploring of the structural metamorphosis can lead to a more comprehensive understanding of such reaction systems and reaction mechanisms, *e.g.*, to the development of novel materials employing solid-state reactions.

The magnetic properties and EPR spectra are determined by the antisymmetric (Dzialoshinskii−Moriya) exchange interactions resulting in abnormally low *g* values ($g_{x,y} < 1$) of the trinuclear species. This may be the first case of observing these low-*g* resonances in the high-frequency EPR. Resonances due to dinuclear and mononuclear entities appear also in the EPR spectra, indicating imperfection of the lattice.

ASSOCIATED CONTENT

Supporting Information

Crystallographic data, experimental details for X-ray structural analyses and spectral characterization data. This material is available free of charge via the Internet at http://pubs.acs.org.

AUTHOR INFORMATION

Corresponding Authors

*E-mail: ab_lysenko@univ.kiev.ua (A.B.L.)
*E-mail: ozarowsk@magnet.fsu.edu (A.O.)

Notes

The authors declare no competing financial interest.

ACKNOWLEDGMENTS

The high-field EPR spectra were recorded at the NHMFL, which is funded by the National Science Foundation (NSF) through the Cooperative Agreement DMR-1157490, the State

of Florida and the Deparetment of Energy (DOE). We are also grateful to the Ministry of Science and Higher Education of Poland for financial support in the purchase of the Bruker ELEXSYS E 500 EPR spectrometer. Financial support from Deutsche Forschungsgemeinschaft and the Ukrainian education program, for the education, training of students, Ph.D. students, scientific and pedagogical staff abroad is gratefully acknowledged.

REFERENCES

(1) Aromí, G.; Barrios, L. A.; Roubeau, O.; Gamez, P. *Coord. Chem. Rev.* **2011**, *255*, 485−546.
(2) (a) Di Nicola, C.; Karabach, Y. Y.; Kirillov, A. M.; Monari, M.; Pandolfo, L.; Pettinari, C.; Pombeiro, A. J. L. *Inorg. Chem.* **2007**, *46*, 221−230. (b) Di Nicola, C.; Garau, F.; Gazzano, M.; Aátima, C.; Guedes da Silva, M.; Lanza, A.; Monari, M.; Nestola, F.; Pandolfo, L.; Pettinari, C.; Pombeiro, A. J. L. *Cryst. Growth Des.* **2012**, *12*, 2890−2901.
(3) Su, S.; Zhang, Y.; Zhu, M.; Song, X.; Wang, S.; Zhao, S.; Song, S.; Yang, X.; Zhang, H. *Chem. Commun.* **2012**, *48*, 11118−11120.
(4) (a) *Magnetic Molecular Materials*; Gatteschi, D., Kahn, O., Miller, J. S., Palacio, F., Eds.; Kluwer Academic: Dordrecht, The Netherlands, 1991. (b) Kahn, O.; Pei. Y.; Yournaux, Y. In *Inorganic Material*; Bruce, D. W., O'Hare, O., Eds.; John Wiley & Sons: Chichester, U.K., 1992. (c) Kahn, O. *Molecular Magnetism*; VCH Publishers: New York, 1993. (d) *Molecule-Based Magnetic Materials: Theory, Techniques, and Applications*; Turnbull, M. M., Sugimoto, T., Thompson, L. K., Eds.; ACS Symposium Series 644; American Chemical Society: Washington, DC, 1996.
(5) Yang, E.-C.; Liu, Z.-Y.; Shi, X.-J.; Liang, Q.-Q.; Zhao, X.-J. *Inorg. Chem.* **2010**, *49*, 7969−7975.
(6) (a) Solomon, E. I.; Sundaram, U. M.; Machonkin, T. E. *Chem. Rev.* **1996**, *96*, 2563−2606. (b) Messerschmidt, A. In *Structure and Bonding*; Hill, H. A. O.; Sadler, P. J., Thomson, A. J., Eds.; Springer: Berlin/Heidelberg, 1998; Vol. *90*, pp 37−68.
(7) (a) Ferrer, S.; Lloret, F.; Pardo, E.; Clemente-Juan, J. M.; Liu-González, M.; García-Granda, S. *Inorg. Chem.* **2012**, *51*, 985−1001. (b) Ferrer, S.; Lloret, F.; Bertomeu, I.; Alzuet, G.; Borrás, J.; García-Granda, S.; Liu-González, M.; Haasnoot, J. G. *Inorg. Chem.* **2002**, *41*, 5821−5830. (c) Ferrer, S.; Haasnoot, J. G.; Reedijk, J.; Müller, E.; Biagini Cingi, M.; Lanfranchi, M.; Manotti Lanfredi, A. M.; Ribas, J. *Inorg. Chem.* **2000**, *39*, 1859−1867. (d) Lider, E. V.; Peresypkina, E. V.; Smolentsev, A. I.; Elokhina, V. N.; Yaroshenko, T. I.; Virovets, A. V.; Ikorskii, V. N.; Lavrenova, L. G. *Polyhedron* **2007**, *26*, 1612−1618. (e) Zhou, J.-H.; Cheng, R.-M.; Song, Y.; Li, Y.-Z.; Chen, X.-T.; Xue, Z.-L.; You, X.-Z. *Inorg.Chem.* **2005**, *44*, 8011−8022. (f) Wu, X.-Y.; Kuang, X.-F.; Zhao, Z.-G.; Chen, S.-C.; Xie, Y.-M.; Yu, R.-M.; Lu, C.-Z. *Inorg. Chim. Acta* **2010**, *363*, 1236−1242. (g) Liu, J.-C.; Guo, G.-C.; Huang, J.-S.; You, X.-Z. *Inorg. Chem.* **2003**, *42*, 235−243. (h) Ferrer, S.; Aznar, E.; Lloret, F.; Castineiras, A.; Liu-Gonzalez, M.; Borras, J. *Inorg. Chem.* **2007**, *46*, 372−374.
(8) (a) Ouellette, W.; Yu, M.-H.; O'Connor, C. J.; Hagrman, D.; Zubieta, J. *Angew. Chem., Int. Ed.* **2006**, *45*, 3497−3500. (b) Yamada, T.; Maruta, G.; Takeda, S. *Chem. Commun.* **2011**, *2*, 653−655. (c) Yang, E.-C.; Liu, Z.-Y.; Wang, X.-G.; Batten, S. R.; Zhao, X.-J. *CrystEngComm* **2008**, *10*, 1140−1143. (d) Huang, X.-C.; Luo, W.; Shen, Y.-F.; Lin, X.-J.; Li, D. *Chem. Commun.* **2008**, *34*, 3995−3997. (e) Ouellette, W.; Prosvirin, A. V.; Chieffo, V.; Dunbar, K. R.; Hudson, B.; Zubieta, J. *Inorg.Chem.* **2006**, *45*, 9346−9366. (f) Ding, B.; Yi, L.; Cheng, P.; Liao, D.-Z.; Yan, S.-P. *Inorg. Chem.* **2006**, *45*, 5799−5803.
(9) (a) Lincke, J.; Lässig, D.; Stein, K.; Moellmer, J.; Kuttatheyil, A. V.; Reichenbach, C.; Moeller, A.; Staudt, R.; Kalies, G.; Bertmer, M.; Krautscheid, H. *Dalton Trans.* **2012**, *41*, 817−824. (b) Lässig, D.; Lincke, J.; Moellmer, J.; Reichenbach, C.; Moeller, A.; Gläser, R.; Kalies, G.; Cychosz, K. A.; Thommes, M.; Staudt, R.; Krautscheid, H. *Angew. Chem., Int. Ed.* **2011**, *50*, 10344−10348. (c) Chen, M.; Chen, M.-S.; Okamura, T.; Lv, M.-F.; Sun, W.-Y.; Ueyama, N. *CrystEngComm* **2011**, *13*, 3801−3810.
(10) (a) Senchyk, G. A.; Lysenko, A. B.; Krautscheid, H.; Rusanov, E. B.; Chernega, A. N.; Krämer, K. W.; Liu, S.-X.; Decurtins, S.; Domasevitch, K. V. *Inorg. Chem.* **2013**, *52*, 863−872. (b) Ling, Y.; Yang, F.; Deng, M.; Chen, Z.; Liu, X.; Weng, L.; Zhou, Y. *Dalton Trans.* **2012**, *41*, 4007−4011. (c) Sarma, D.; Srivastava, V.; Natarajan, S. *Dalton Trans.* **2012**, *41*, 4135−4145. (d) Ren, H.; Song, T.-Y.; Xu, J.-N.; Jing, S.-B.; Yu, Y.; Zhang, P.; Zhang, L.-R. *Cryst. Growth Des.* **2009**, *9*, 105−112. (e) Wang, X.-L.; Qin, C.; Lan, Y.-Q.; Shao, K.-Z.; Su, Z.-M.; Wang, E.-B. *Chem. Commun.* **2009**, *4*, 410−412. (f) Park, H.; Moureau, D. M.; Parise, J. B. *Chem. Mater.* **2006**, *18*, 525−531. (g) Hulvey, Z.; Falcao, E. H. L.; Eckert, J.; Cheetham, A. K. *J. Mater. Chem.* **2009**, *19*, 4307−4309. (h) Yang, E.-C.; Liang, Q.-Q.; Wang, P.; Zhao, X.-J. *Inorg. Chem. Commun.* **2009**, *12*, 211−213. (i) Mahata, P.; Prabu, M.; Natarajan, S. *Cryst. Growth Des.* **2009**, *9*, 3683−3691. (j) Zhai, Q.-G.; Lu, C.-Z.; Wu, X.-Y.; Batten, S. R. *Cryst. Growth Des.* **2007**, *7*, 2332−2342. (k) Luo, F.; Che, Y.-X.; Zheng, J.-M. *CrystEngComm* **2009**, *11*, 1097−1102. (l) Chowdhuri, D. S.; Rana, A.; Bera, M.; Zangrando, E.; Dalai, S. *Polyhedron* **2009**, *28*, 2131−2136. (m) Habib, H. A.; Sanchiz, J.; Janiak, C. *Dalton Trans.* **2008**, *13*, 1734−1744. (n) Senchyk, G. A.; Lysenko, A. B.; Krautscheid, H.; Sieler, J.; Domasevitch, K. V. *Acta Crystallogr.* **2008**, *C64*, m246−m249.
(11) Naik, A. D.; Dîrtu, M. M.; Léonard, A.; Tinant, B.; Marchand-Brynaert, J.; Su, B.-L.; Garcia, Y. *Cryst. Growth Des.* **2010**, *10*, 1798−1807.
(12) Lässig, D.; Lincke, J.; Gerhardt, R.; Krautscheid, H. *Inorg. Chem.* **2012**, *51*, 6180−6189.
(13) Xia, B.; Chen, Z.; Zheng, Q.; Zheng, H.; Deng, M.; Ling, Y.; Weng, L.; Zhou, Y. *CrystEngComm* **2013**, *15*, 3484−3489.
(14) (a) Bartlett, R. K.; Humphrey, I. R. *J. Chem. Soc.* **1967**, *C17*, 1664−1666. (b) Bondar, O. A.; Lukashuk, L. V.; Lysenko, A. B.; Krautscheid, H.; Rusanov, E. B.; Chernega, A. N.; Domasevitch, K. V. *CrystEngComm* **2008**, *10*, 1216−1226.
(15) Sheldrick, G. M. *Acta Crystallogr.* **2008**, *A64*, 112−122.
(16) Spek, A. L. *J. Appl. Crystallogr.* **2003**, *36*, 7−13.
(17) (a) O'Connor, C. J. *Prog. Inorg. Chem.* **1982**, *29*, 203−283. (b) Bain, G. A.; Berry, J. F. *J. Chem. Educ.* **2008**, *85*, 532−536.
(18) Hassan, A. K.; Pardi, L. A.; Krzystek, J.; Sienkiewicz, A.; Goy, P.; Rohrer, M.; Brunel, L.-C. *J. Magn. Reson.* **2000**, *142*, 300−312.
(19) Naik, A. D.; Marchand-Brynaert, J.; Garcia, Y. *Synthesis* **2008**, *1*, 149−154.
(20) Lysenko, A. B.; Govor, E. V.; Krautscheid, H.; Domasevitch, K. V. *Dalton Trans.* **2006**, *31*, 3772−3776.
(21) (a) Blatov, V. A. *IUCr CompComm Newsletter* **2006**, *7*, 4−38. (b) Blatov, V. A.; Shevchenko, A. P.; Serezhkin, V. N. *J. Appl. Crystallogr.* **2000**, *33*, 1193−1193.
(22) (a) Holliday, B. J.; Mirkin, C. A. *Angew. Chem., Int. Ed.* **2001**, *40*, 2022−2043. (b) Seidel, S. R.; Stang, P. J. *Acc. Chem. Res.* **2002**, *35*, 972−983. (c) Swiegers, G. F.; Malefetse, T. J. *Coord. Chem. Rev.* **2002**, *225*, 91−102. (d) Cotton, F. A.; Lin, C.; Murillo, C. A. *Acc. Chem. Res.* **2001**, *34*, 759−771.
(23) (a) MacGillivray, L. R.; Atwood, J. L. *Angew. Chem., Int. Ed.* **1999**, *38*, 1018−1033. (b) Moulton, B.; Zaworotko, M. J. *Chem. Rev.* **2001**, *101*, 1629−1658. (c) Perry, J. J., IV; Perman, J. A.; Zaworotko, M. J. *Chem. Soc. Rev.* **2009**, *38*, 1400−1417.
(24) Wang, Y.; Cheng, P.; Song, Y.; Liao, D.-Z.; Yan, S.-P. *Chem.—Eur. J.* **2007**, *13*, 8131−8138.
(25) Senchyk, G. A.; Lysenko, A. B.; Rusanov, E. B.; Chernega, A. N.; Jezierska, J.; Domasevitch, K. V.; Ozarowski, A. *Eur. J. Inorg. Chem.* **2012**, 5802−5813.
(26) Moriya, T. *Phys. Rev.* **1960**, *120*, 91−98.
(27) Yoon, J.; Solomon, E. I. *Coord. Chem. Rev.* **2007**, *251*, 379−400.
(28) Neese, F. *ORCA: An ab Initio, Density Functional and Semiempirical Program Package*, version 2.9.1; 2012, free download from http://www.cec.mpg.de/forum/downloads.php.
(29) Neese, F. *Wiley Interdiscip. Rev.: Comput. Mol. Sci.* **2012**, *2*, 73−78.
(30) (a) Schaefer, A.; Horn, H.; Ahlrichs, R. *J. Chem. Phys.* **1992**, *97*, 2571−2577. (b) The Ahlrichs auxiliary basis sets were obtained from

the *TurboMole* basis set library under ftp.chemie.uni-karlsruhe.de/pub/jbasen. (c) Eichkorn, K.; Treutler, O.; Ohm, H.; Haser, M.; Ahlrichs, R. *Chem. Phys. Lett.* **1995**, *240*, 283−290. (d) Eichkorn, K.; Weigend, F.; Treutler, O.; Ahlrichs, R. *Theor. Chem. Acc.* **1997**, *97*, 119−124.
(31) (a) Becke, D. A. *Phys. Rev. A* **1988**, *38*, 3098−3100. (b) Perdew, J. P. *Phys. Rev. B* **1986**, *33*, 8822−8824. (c) Perdew, J. P. *Phys. Rev. B.* **1986**, *34*, 7406−7406. (c) Kendall, R. A.; Früchtl, H. A. *Theor. Chem. Acc.* **1997**, *97*, 158−163.